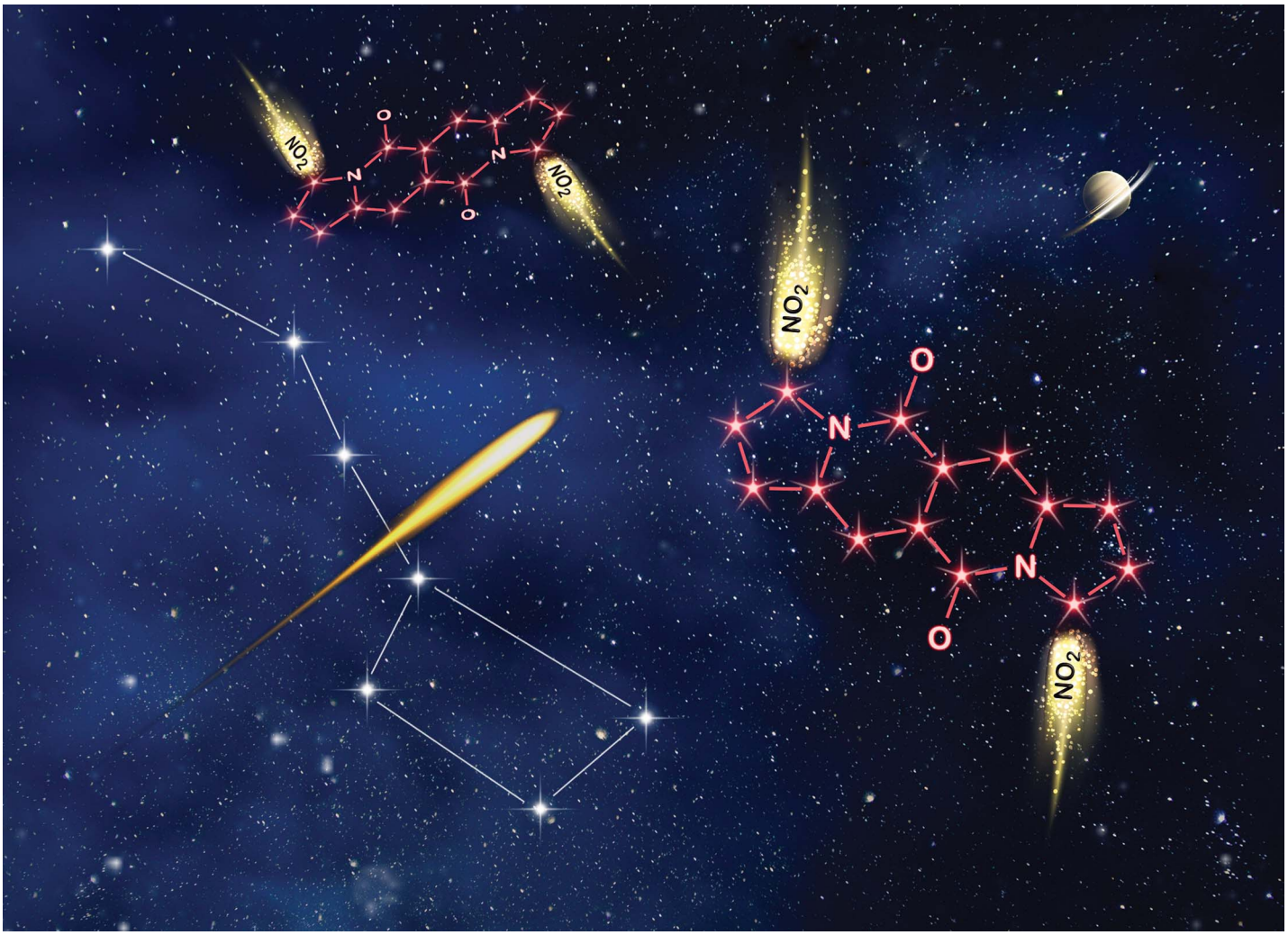

Showcasing research from Professor Gryko's laboratory, Polish Academy of Sciences, Institute of Organic Chemistry, Poland.

Potent strategy towards strongly emissive nitroaromatics through a weakly electron-deficient core

A new strategy towards strongly fluorescent nitroaromatics was discovered. The design relies on linking an electron-deficient dipyrrolonaphthyridinedione core with nitro groups through biaryl linkage. This strategy of preventing the known processes that compete with photoemission leads to the emergence of unprecedented alternative mechanisms for fluorescence quenching, involving transitions to dark nπ* singlet states and aborted photochemistry. When conical intersections interrupt the trajectories of these reactions, internal conversion leads to restoration of the initial ground state and molecular structure.

As featured in:

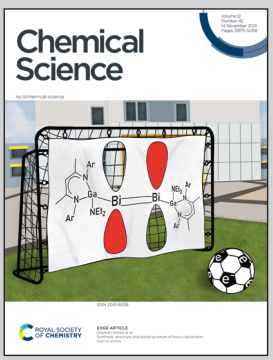

See Daniel T. Gryko *et al.*, *Chem. Sci.*, 2021, **12**, 14039.

ROYAL SOCIETY OF CHEMISTRY

rsc.li/chemical-science

Registered charity number: 207890

Chemical Science

ROYAL SOCIETY OF CHEMISTRY

EDGE ARTICLE

View Article Online
View Journal | View Issue

Cite this: *Chem. Sci.*, 2021, **12**, 14039

All publication charges for this article have been paid for by the Royal Society of Chemistry

Potent strategy towards strongly emissive nitroaromatics through a weakly electron-deficient core†

Bartłomiej Sadowski, ‡[a] Marzena Kaliszewska,[b] Yevgen M. Poronik, [a] Małgorzata Czichy,[c] Patryk Janasik, [c] Marzena Banasiewicz,[d] Dominik Mierzwa,[a] Wojciech Gadomski, [b] Trevor D. Lohrey, [ef] John A. Clark, [g] Mieczysław Łapkowski,*[c] Bolesław Kozankiewicz, *[d] Valentine I. Vullev, *[ghij] Andrzej L. Sobolewski, *[d] Piotr Piatkowski *[b] and Daniel T. Gryko *[a]

Received 6th July 2021
Accepted 5th September 2021

DOI: 10.1039/d1sc03670j

rsc.li/chemical-science

Nitroaromatics seldom fluoresce. The importance of electron-deficient (n-type) conjugates, however, has inspired a number of strategies for suppressing the emission-quenching effects of the strongly electron-withdrawing nitro group. Here, we demonstrate how such strategies yield fluorescent nitroaryl derivatives of dipyrrolonaphthyridinedione (DPND). Nitro groups near the DPND core quench its fluorescence. Conversely, nitro groups placed farther from the core allow some of the highest fluorescence quantum yields ever recorded for nitroaromatics. This strategy of preventing the known processes that compete with photoemission, however, leads to the emergence of unprecedented alternative mechanisms for fluorescence quenching, involving transitions to dark nπ* singlet states and aborted photochemistry. Forming nπ* triplet states from ππ* singlets is a classical pathway for fluorescence quenching. In nitro-DPNDs, however, these ππ* and nπ* excited states are both singlets, and they are common for nitroaryl conjugates. Understanding the excited-state dynamics of such nitroaromatics is crucial for designing strongly fluorescent electron-deficient conjugates.

Introduction

The nitro group is well known for its ability to quench fluorescence when appended to a fluorophore skeleton.[1–5] It effectively reduces the emission brightness from one- and two-photon excitation – a crucial consideration for the design and implementation of fluorescent probes for biomedical imaging.[6,7] Nevertheless, the immense electron-withdrawing strength of the nitro group makes it a highly attractive substituent for the pursuit of electron-deficient, *i.e.*, n-type, organic conjugates and potent photooxidants.[8–11] Decoupling the nitro substituents from the states involved in radiative transitions leads to fluorescence with substantial quantum yields (Φ_{fl}) (Fig. 1A);[12,13] however, such a strategy negates the benefits that may be gained from the electron-withdrawing strength of this substituent.

Despite their importance, many aspects of the relationship between molecular structure and fluorescence intensity of nitroaromatics still remain puzzling. For a wide range of simple nitro-containing derivatives, such as nitrobenzene,[14] 1-nitropyrene,[15] 1-nitronaphthalene,[16] and 9-nitroanthracene,[17] triplet manifolds, *i.e.*, intersystem crossing (ISC), present the most common pathway for energy dissipation, leading to a drastic decrease in the lifetimes of the fluorescent excited states. Conversely, the strongly electron-withdrawing nitro group induces a charge-transfer (CT) character in the excited states,

[a]*Institute of Organic Chemistry, Polish Academy of Sciences, Kasprzaka 44/52, 01-224 Warsaw, Poland. E-mail: dtgryko@icho.edu.pl*
[b]*Faculty of Chemistry, University of Warsaw, Zwirki i Wigury 101, 02-089 Warsaw, Poland. E-mail: piatek@chem.uw.edu.pl*
[c]*Faculty of Chemistry, Silesian University of Technology, Strzody 9, 44-100 Gliwice, Poland. E-mail: mieczyslaw.lapkowski@polsl.pl*
[d]*Institute of Physics, Polish Academy of Sciences, Aleja Lotnikow 32/46, 02-668 Warsaw, Poland. E-mail: sobola@ifpan.edu.pl; kozank@ifpan.edu.pl*
[e]*Department of Chemistry, University of California, Berkeley, 420 Latimer Hall, Berkeley, CA, USA*
[f]*Chemical Sciences Division, Lawrence Berkeley National Laboratory, 1 Cyclotron Road, Berkeley, CA, USA*
[g]*Department of Bioengineering, University of California, Riverside, 900 University Ave., Riverside, CA 92521, USA. E-mail: vullev@ucr.edu*
[h]*Department of Chemistry, University of California, Riverside, 900 University Ave., Riverside, CA 92521, USA*
[i]*Department of Biochemistry, University of California, Riverside, 900 University Ave., Riverside, CA 92521, USA*
[j]*Materials Science and Engineering Program, University of California, Riverside, 900 University Ave., Riverside, CA 92521, USA*

† Electronic supplementary information (ESI) available. CCDC 2019018–2019020. For ESI and crystallographic data in CIF or other electronic format see DOI: 10.1039/d1sc03670j

‡ Present address: Institut für Organische und Biomolekulare Chemie, Georg-August-Universität, Tammannstrasse 2, 37077 Göttingen, Germany.

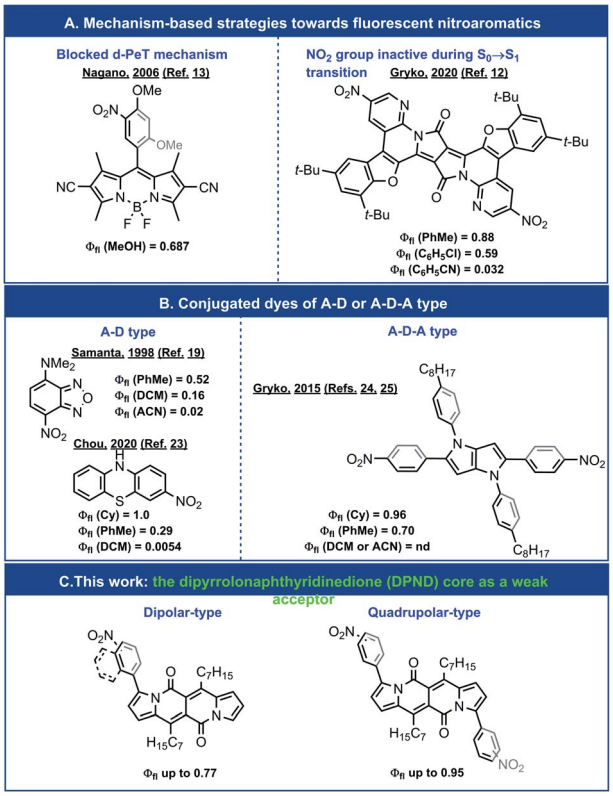

Fig. 1 Exemplary highly emissive nitroaromatics. A – an acceptor moiety containing NO_2 group. D – a donor moiety. nd – not detected.

which tends to reduce the rate of ISC.[18] In fact, for about half a century, amine derivatives of nitrobenzodioxazole (NBD) have been favoured as small fluorescent probes for biological samples (Fig. 1B).[19,20] A recent expansion of the variety of amino-NBD analogues widens their working range to the near infrared spectral region.[21] Expanding this push–pull strategy to other nitroaromatics can also result in some observable fluorescence (Fig. 1B).[22,23]

Inducing a CT character in the excited states, however, presents an alternative set of challenges. (1) An increase in the CT character, usually accompanied by dihedral twisting, can spatially separate the natural transition orbitals (NTOs), which decreases the oscillator strength of the radiative decays to negligibly low values and renders such CT states dark. (2) Medium polarity stabilizes polar CT states and brings them closer to the potential-energy surface (PES) of the ground state, which opens pathways for efficient deactivation *via* internal conversion (IC). These features warrant tuning of the CT character of the excited states in order to balance its benefits with the limitations it imposes.

Transferring this strategy for dipolar donor–acceptor (D–A) conjugates to chromophores with quadrupolar symmetry, *e.g.*, acceptor–donor–acceptor (A–D–A) structures, presents an alternative paradigm for fluorescent nitroaromatics.[24] In addition to their importance for non-linear optical applications, quadrupolar dyes tend to manifest pronounced solvatofluorochromism.[24–28] That is, medium polarity has no effect on their absorption maxima because of the quadrupolar ground-state symmetry, while CT upon photoexcitation leads to symmetry breaking, leading to dipolar fluorescent states and polarity-induced bathochromic shifts of the emission.[29] This property is crucially beneficial for imaging where the excitation wavelength is invariant to the media, while the fluorescence acts as a reporter for the polarity of the surrounding microenvironment.

For A–D–A dyes, tuning the coupling between electron-donating chromophore cores (D) and the nitro groups, which are components of the acceptors (A), allows for quantitative Φ_{fl} in solvents with low polarity.[24] Media with even moderate polarity, such as dichloromethane (DCM), however, quenches the fluorescence of these nitroaromatic dyes.[24]

We sought, and now report, an effective approach to improving the emission properties of fluorophores containing nitro groups. In addition to tuning the electronic coupling of the core with the nitro groups, we focus on the utility of weakening the electron donor in D–A and A–D–A dyes. Our design of a series of nitroaromatic D–A and A–D–A conjugates comprise a weakly electron-donating dipyrrolonaphthyridinedione[30] (DPND) as a core (Fig. 1C). In addition to the high Φ_{fl} values that we observe in DCM, many of these nitro-DPND conjugates fluoresce even in polar solvents, such as acetonitrile (ACN). Theoretical analysis reveals that for about half of these dyes, a low-lying $n\pi^*$ singlet state, rather than a dark CT state, provides pathways for IC. Also, the dihedral twisting along the PES of the lowest singlet excited state accompanies the formation of a new bond that breaks after the IC transition to the ground state. Despite the years of discussion and hypotheses about such transient covalent interactions along excited-state reaction pathways,[31,32] it was only recently that experimental proof for such processes became possible to obtain for relatively simple structures.[33,34] Mechanisms involving these types of aborted photochemical reactions are unprecedented in the study of deactivation pathways in photoexcited nitroaromatics. Along with the observed fluorescence for polar media, this result presents a key consideration in the pursuit of n-type organic materials and photooxidants.

Results and discussion

Design and synthesis

DPNDs are a series of cross-conjugated heterocyclic chromophores with unique photophysical and electrochemical properties that allow them to act as week electron donors or weak electron acceptors,[30,35–37] making them an excellent choice for designing the D–A and A–D–A conjugates for this study. Biaryl-like linkages enable weak coupling between the nitro group(s) and the DPND core (Fig. 2). Pd-catalyzed direct arylation[35] of DPND **1** with the corresponding aryl bromides allows us to obtain the D–A and A–D–A conjugates with nitro groups at *ortho*, *meta*, *para* and *peri* positions with respect to the core (see ESI† for synthetic details). This shift in the position of the nitro groups varies their electronic coupling with the DPND moiety.

X-ray crystallography for DPNDs **7**, **9** and **12** unambiguously shows twisted conformations of the constructed dyes (Fig. S1,

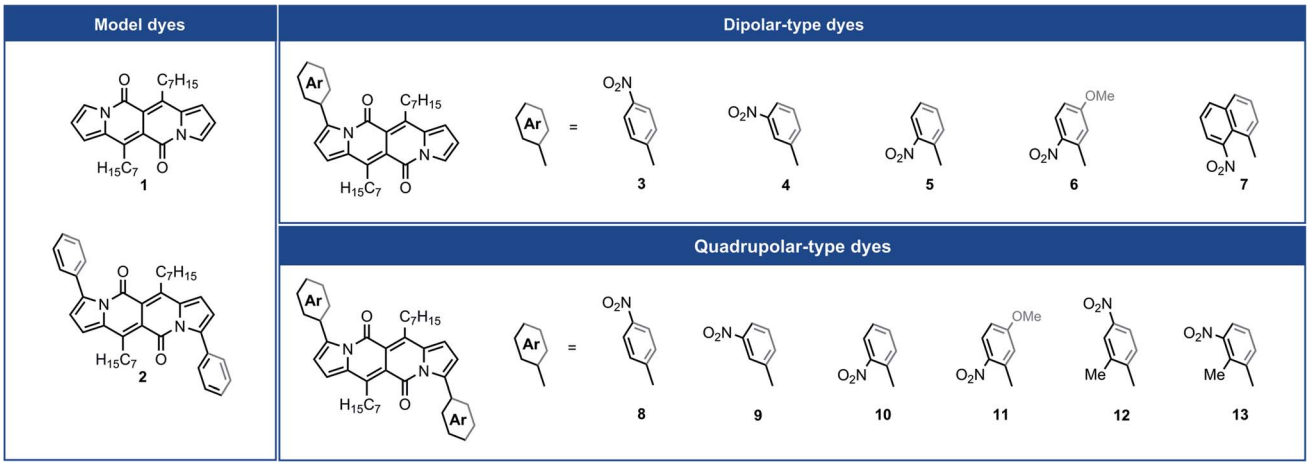

Fig. 2 The molecular structures of DPNDs considered in this work.

S2 and Table S1 in ESI†). The average dihedral angles between adjacent aryl moieties in **9** and **12** are 51.6° and 56.1°, respectively. These values are slightly smaller than that for **2** (58.9°),[38] suggesting planarity-inducing weak electronic communication between the nitro-enriched aryls and the DPND core.

Steady-state optical absorption and emission

Four aprotic solvents, *n*-hexane (HEX), 1,2-dichlorobenzene (DCB), dichloromethane (DCM), and acetonitrile (ACN), allowed for the exploration of the effects of medium polarity on the optical properties of the DPNDs **1–13** (Fig. 3, Table S2, and Fig. S3–S15†). In addition, we employed two ester solvents, propyl butyrate (PB) and sucrose octaacetate (SOA), for testing the effects of medium viscosity on the spectral properties of the analysed dyes.[39]

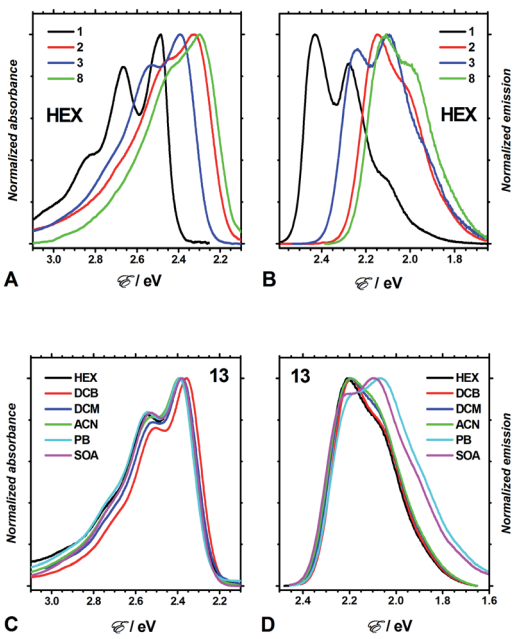

Fig. 3 Optical absorption and emission spectra of DPND dyes for various solvents. (A and B) Absorption and fluorescence spectra of **1**, **2**, **3** and **8** for hexane (λ_{ex} = 450 nm for **1** and **2**; 480 nm for **3**; and 510 nm for **8**). (C and D) Solvent dependence of the absorption and fluorescence spectra of **13** (λ_{ex} = 470 nm for HEX; and 505 nm for the rest of the solvents).

Consistent with extension of the π-conjugated framework, substitution of the DPND core with peripheral phenyl or nitrophenyl groups bathochromically shifts the absorption and emission maxima (Fig. 3A, B, 4A and B). The absorption and emission maxima (E_{abs} and E_{fl}, respectively) of the dinitrophenyl conjugates, *i.e.*, **8–13**, cluster around those of **2** for each of the solvents (Fig. 4B). The spectral maxima of the *para*-nitro, **8**, and *ortho*-nitro, **10** and **11**, conjugates are similar or bathochromically shifted in comparison with those of **2**. Conversely, E_{abs} and E_{fl} of the *meta*-nitro dyes, **9** and **13**, are larger than those of **2** (Fig. 4B). These findings correlate with donor–acceptor electronic coupling between *meta* substituents that is weaker than that between *para* and *ortho* ones.[40] Placing methyl groups at the *ortho* positions, such as in **12** and **13**, causes hypsochromic shifts in comparison with the non-methylated analogues, **8** and **9**, respectively (Fig. 4B). These data are consistent with a sterically-induced increase in the dihedral between nitrophenyl and the DPND core, which decreases their electronic coupling.

The spectral maxima of the mono-nitrophenyl DPNDs show similar trends (Fig. 4A). In comparison to the mono- and di-*ortho*-nitrophenyl conjugates, **5** and **10**, adding methoxy substituents at *para*-positions relative to the nitro groups, as in **6** and **11**, causes slight hypsochromic shifts (Fig. 4A and B). This suggests a weakening of the effects of the nitro groups induced by the electron-donating ones. This weakening effect can also provide a plausible explanation for the deviated optical behaviour of **13**, *i.e.*, **13** displays the most hypsochromic spectral maxima among the di-nitrophenyl DPNDs (Fig. 4B). Namely, methyls are weakly electron-donating, which may lessen the effect of the nitro groups in **13**.

These solvent effects are quite similar for all dyes **1–13** (Fig. 4A and B). Hence, attaching nitroaryl substituents to the DPND core does not enhance the polarity effects on the energy gaps between the ground and excited states involved in the radiative transitions.

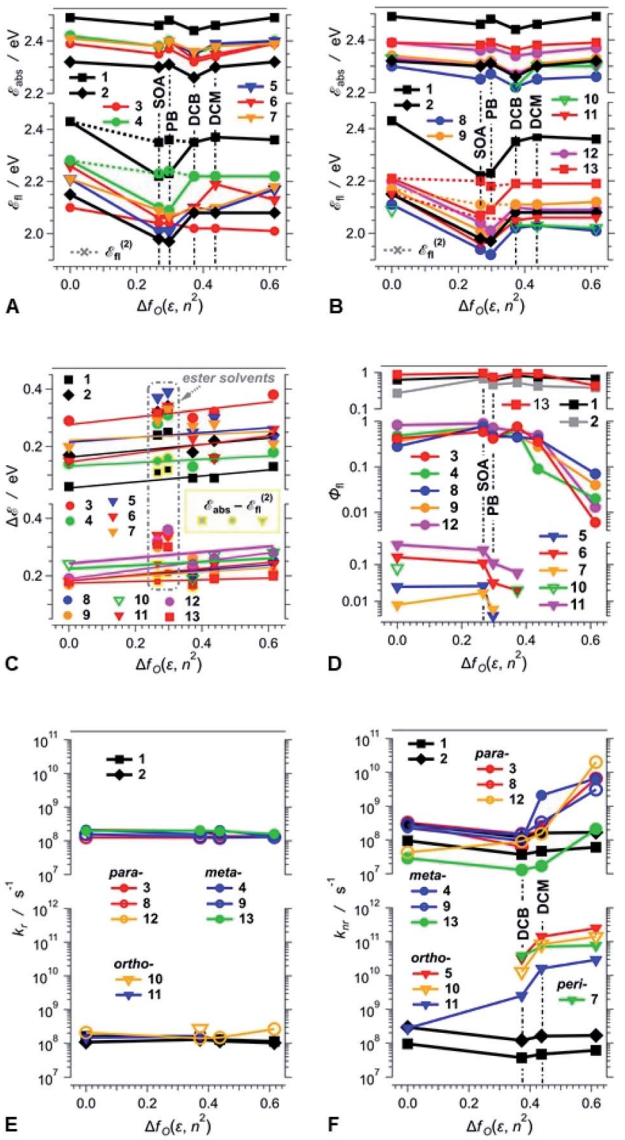

Fig. 4 Dependence of the photophysical properties of the DPND dyes on the solvent polarity expressed in terms of the Onsager function, $f_O(x) = 2(x-1)/(2x+1)$, $f_O(\varepsilon, n^2) = f_O(\varepsilon) - f_O(n^2)$. (A and B) Dependence of the absorption and emission maxima, E_{abs} and E_{fl}, respectively, on $f_O(\varepsilon, n^2)$. For the ester solvents, PB and SOA, the conversion of the fluorescence spectra from wavelength to energy scales, *i.e.*, $F(E) = F(\lambda)E^{-5}$, shifts the order of the vibronic maxima, *i.e.*, the highest (hypsochromically positioned) peaks in a wavelength scale becomes the second highest, $E_{fl}^{(2)}$, in an energy scale. The dotted lines connect with $E_{fl}^{(2)}$ for PB and SOA. (C) Polarity effects on the Stokes' shifts, $\Delta E = E_{abs} - E_{fl}$. For PB and SOA, The yellow-framed markers represent the Stokes' shifts calculated using $E_{fl}^{(2)}$. The lines represent the best linear fits of ΔE *vs.* $f_O(\varepsilon, n^2)$ for HEX, DCB, DCM and ACN. (D) Polarity effects on the fluorescence quantum yields, Φ_{fl}. (E and F) Polarity dependence of the radiative, k_r, and non-radiative, k_{nr}, rate constants estimated from the fluorescence quantum yields and the excited-state lifetimes (τ) for samples manifesting $\Phi_{fl} > 10^{-4}$, *i.e.*, $k_r = \Phi_{fl}\tau^{-1}$ and $k_{nr} = (1 - \Phi_{fl})\tau^{-1}$. For weakly fluorescent compounds, *i.e.*, $(1 - \Phi_{fl}) \approx 1$, $k_{nr} \approx \tau^{-1}$.

An increase in medium polarity slightly increases the Stokes' shifts (ΔE) of the DPNDs (Fig. 4C), indicating that the fluorescent S_1 state is more polarized than the relaxed ground state. The slopes of the linear fits of ΔE *vs.* $f_O(\varepsilon, n^2)$, however, are relatively small. Lippert–Mataga–Ooshika analysis[41–43] reveals that the difference between the electric dipole moments, $\Delta\mu$, of the S_0 and the fluorescent excited states is about 2 D for dyes **4**, **5**, **7** and **13**, containing nitro groups on the *ortho* or *meta* positions, which is similar to $\Delta\mu$ for the DPND **1** with no aryl substituents (Table S4†). On the other hand, dyes with two phenyl or *para*-nitrophenyl substituents (**2**, **8**, **11** and **12**) exhibit $\Delta\mu$ values between 4 and 6 D. These values of $\Delta\mu$ are consistent with a breaking of ground-state quadrupole electronic symmetry and the formation of dipolar excited states. Considering the relatively large size of these molecules, $\Delta\mu$ values of 2 to 6 D, corresponding to 0.4 to 1.2*e* Å, do not indicate well-defined charge separation. The nitroaryl substituents, therefore, do not appear to induce a significant CT character in the emissive S_1 states of the DPNDs under study.

Three distinct patterns of behaviour emerge from the polarity effects on the fluorescence quantum yields of the DPND dyes (Fig. 4D):

First, the fluorescence quantum yields of **1**, **2** and **13** are relatively large, *i.e.*, between 0.3 and 1, and show no correlation with solvent polarity (Fig. 4D). The lack of marked solvent effects on the optical properties of **13** is consistent with its structure: (1) the nitro groups are at the *meta* positions of the phenyl substituents, causing weakened coupling with the DPND core, (2) the *ortho* methyl groups enhance the dihedral angles, further decreasing the coupling, and (3) the electron-donating methyls also dampen the effect of the nitro groups. Therefore, **13** behaves similarly to the DPNDs without nitroaryl substituents, exhibiting exceptionally large Φ_{fl} even for polar media, *i.e.*, Φ_{fl} of **13** for DCM and ACN is 0.92 and 0.43, respectively.

Second, when in non-polar media, **3**, **4**, **8**, **9** and **12** are strongly fluorescent with $\Phi_{fl} \gtrsim 0.3$ (Fig. 4D). As the solvent polarity increases beyond that of DCB, Φ_{fl} drops by an order of magnitude or more (Fig. 4D). This behaviour of the DPNDs with *para* and *meta* nitro groups is consistent with a polarity-induced transition to a dark state that provides pathways for non-radiative deactivation.

Third, the DPND derivatives **5**, **6**, **7**, **10** and **11**, with *ortho* or *peri* nitro groups on their aryl substituents, are weakly fluorescent even in non-polar media (Fig. 4D). An increase in solvent polarity makes their emission barely detectable and their fluorescence quantum yields unquantifiable. This fluorescence quenching is usual for chromophores with 2-nitrophenyl substituents.[24] It is clear that placing the nitro groups at the *ortho* and *peri* positions next to the DPND core provides: (1) efficient pathways for intersystem crossing, as we previously described and (2) through-space pathways for forward and back CT that can efficiently deactivate the S_1 to the S_0 state. While the former can account for the weak fluorescence in the non-polar solvents, the latter is consistent with polarity-induced emission quenching.

Comparison between the results obtained in liquid PB *versus* solid SOA reveals that the medium viscosity has a small impact on the photophysics of the DPNDs (Fig. 4 and Table S2†). The values of Φ_{fl} for SOA are larger than those for PB (Table S2†). For the mono-substituted *ortho* and *peri* derivatives, **5**, **6** and **7**, Φ_{fl}

for SOA exceeds Φ_{fl} for PB by a factor of approximately three to seven. For all *meta* and *para* conjugates, on the other hand, these differences between Φ_{fl} for SOA and PB are smaller than a factor of two, which is on par with the trends observed for **1** and **2**, which do not contain nitro groups (Table S2†). These results show that nitro groups at *ortho* or *peri* positions enhance the susceptibility of the DPNDs toward medium viscosity. Nevertheless, these viscosity effects are considerably smaller than those observed as a function of the solvent polarity.

Nanosecond time-resolved emission spectroscopy

Time-correlated single photon counting (TCSPC) reveals mono-exponential nanosecond emission decays for all samples with relatively large Φ_{fl} (Fig. 5). This feature suggests the presence of a single fluorescent species in each of the samples.

All compounds show quite similar radiative-decay rate constants (k_r) with values clustering around 10^8 s^{-1} that are invariant with medium polarity (Fig. 4E). For the non-radiative-decay rate constants (k_{nr}) of the nitroaryl DPNDs, on the other hand, medium polarity induces up to a three orders of magnitude increase, while k_{nr} of **1** and **2** exhibit negligible solvent dependence (Fig. 4F). Among them, the *ortho*- and *peri*-nitroaryl DPNDs, such as **5**, **7**, **10** and **11**, exhibit k_{nr} of about 10^{11} s^{-1} and larger in polar media (Fig. 4F). Even for **13**, where the coupling of the nitro groups with the core is weak, k_{nr} increases by an order of magnitude upon transition from a non-polar to polar solvent (Fig. 4F). These findings unequivocally show that the non-radiative decay rates govern the photophysical trends observed for these DPNDs.

The substantial enhancements of k_{nr} by solvent polarity are consistent with transitions to dark, polarized states that provide pathways for non-radiative deactivation. The susceptibility of k_{nr} for the *ortho*- and *peri*-nitro derivatives, *i.e.*, **5**, **6**, **7**, **10** and **11**, to solvent polarity is considerably stronger than that for the *para*- and *meta*-nitro ones, *i.e.*, **3**, **4**, **8**, **9**, **12** and **13**. This solvent dependence of k_{nr} suggests that the dark states of **5**, **6**, **7**, **10** and **11** are more polarized than those of **3**, **4**, **8**, **9**, **12** and **13**. Therefore, such dark states of the *ortho*- and *peri*-nitro DPNDs most plausibly have a pronounced CT character. Conversely, we cannot unequivocally claim a well-defined CT character for the dark states of the *para*- and *meta*-nitro derivatives.

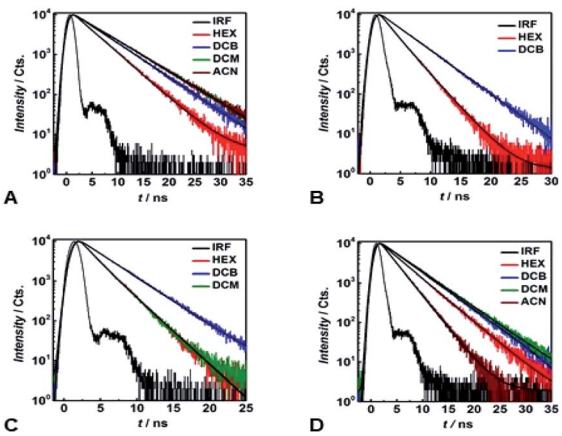

Fig. 5 Emission decays of (A) **1**, (B) **4**, (C) **9** and (D) **13** in various solvents (λ_{ex} = 460 nm; the decays are recorded at λ_{em}, corresponding to the fluorescence maxima; IRF = instrument response function, representing the temporal profile of the excitation pulse, which is recorded by monitoring the Rayleigh scattering of non-fluorescent media at $\lambda_{em} = \lambda_{ex}$). Black solid lines represent monoexponential fits of the experimental data.

Transient-absorption spectroscopy

We conducted pump-probe TA studies on DCB, DCM and ACN solvent media, with sample concentrations required to exceed about 10 times those employed for the fluorescence measurements. Each of the TA spectra of the thirteen DPNDs shows four main features (Fig. 6): (1) a band with negative ΔA around 530 to 550 nm, ascribed to ground-state bleaching (B); (2) a broad band

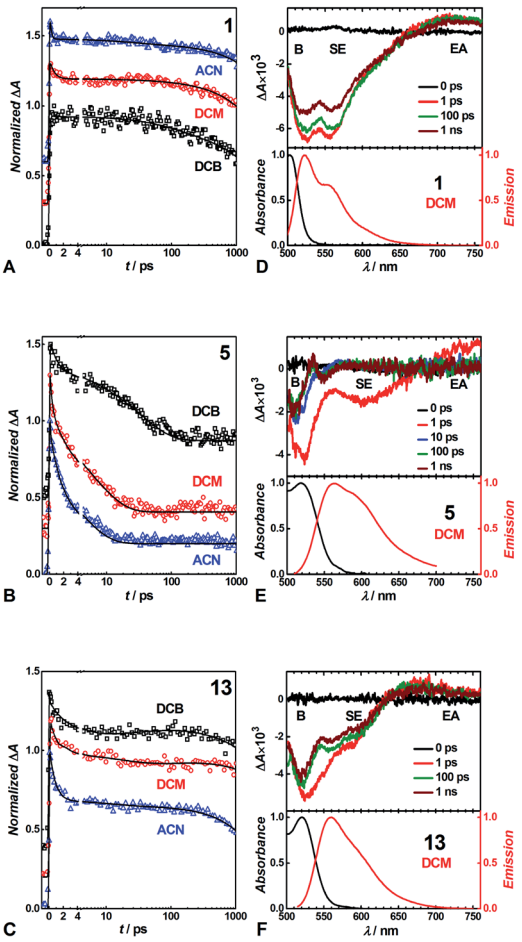

Fig. 6 Transient absorption decays normalized to 1 of (A) **1**, (B) **5** and (C) **13** in different solvents at observation wavelength of 520 nm. Transient absorption spectra at different pump-probe time delays (upper panel) and time-integrated absorption and emission spectra normalized to 1 (lower panel) of (D) **1**, (E) **5** and (F) **13** in DCM. The transient absorption signals were recorded upon excitation at 480 nm. Solid lines are from global multiexponential fits to the experimental data. For clarity the transient absorption decays were offset on the *y*-axis. B – bleach band, SE – stimulated emission, EA – excited state absorption.

between about 550 and 700 nm, also with negative ΔA, ascribed to stimulated emission (SE), as suggested by its overlap with the fluorescence spectra; (3) a weak broad TA band in the red-NIR spectral region (λ >650 nm), ascribed to electronic absorption (EA) involving $S_1 \rightarrow S_n$ transitions; and (4) a TA band at around 550 to 600 nm that the global-fit (GF) analysis makes especially apparent (Fig. 7).

Despite the similarities in the spectral shapes, the TA dynamics vary widely among the different dyes and solvents, as GF analysis reveals. The nanosecond lifetimes obtained from TCSPC, along with two additional picosecond exponential terms, describe well the TA dynamics of the dyes (Table S3†). In all cases, sub-picosecond or picosecond lifetimes, τ_1, smaller than 6 ps, characterize the fastest of the components. These fast transitions reveal the emergence of a 550–600 nm TA band that overlaps with the B and the SE signals, while completely or partially maintaining the red-NIR absorption (Fig. 6 and 7). A bathochromic shift in the SE band can also induce a decrease in ΔA in the red-NIR spectral region. These (sub-)picosecond transitions are consistent with the relaxation of the Franck–Condon (FC) states to the fluorescent S_1 structures. That is, the red-NIR broad TA, along with the SE characterize the FC states. Conversely, the 550–600 nm absorption band, along with bathochromically shifted emission and the same red-NIR TA, originate from the relaxed S_1 state that undergoes radiative deactivation.

For the strongly fluorescent **1**, **2** and **13**, as well as for **3**, **4**, **8**, **9** and **12** in low-polarity solvents, τ_2 represents intermediate lifetimes, ranging between about 20 and 130 ps, which correspond to minute changes in the spectra of the relaxed emissive S_1 state. Most of these changes encompass a small growth of the 550–600 nm TA band or a slight SE bathochromic shift (Fig. 7A–D). Along with the fast (sub-)picosecond components, these intermediate τ_2 lifetimes suggest a degree of heterogeneity in the kinetics of relaxation to the emissive S_1 states. Furthermore, solvent polarity induces a decrease in these intermediate lifetimes (Table S3†), which is consistent with the fluorescent S_1 states tending to be more polar than the S_0 as revealed by Lippert–Mataga–Ooshika analysis (Fig. 4C).

The longest lifetimes, *i.e.*, τ_3 obtained from triexponential fits and τ_2 – from biexponential ones, characterize the decays of the emissive S_1 states: these are the most important values for understanding the fluorescence properties of these dyes. The slowest decays of the *para*- and *meta*-nitro derivatives, along with those of **1** and **2**, represent transitions solely to S_0. For **1**, **2** and **13**, solvent polarity does not truly affect τ_3 (Table S3†). This observation is consistent with minimal to no involvement of CT in the $S_1 \rightarrow S_0$ transitions, which is valid even for **13**, where the nitro groups are quite decoupled from the DPND core.

For the *para* and the other *meta*-substituted DPNDs, on the other hand, an increase in solvent polarity accelerates the $S_1 \rightarrow S_0$ decays. This trend is especially pronounced in ACN, which produces S_1 lifetimes of about 50–300 ps, *i.e.*, significantly shorter than the nanosecond ones observed in HEX or DCB (Table S3†). This drastic decrease in the S_1 lifetimes originates from a polarity-induced increase in k_{nr} for these compounds (Fig. 4F). These results are consistent with a $S_1 \rightarrow S_0$ transition through a short-lived dark CT state. Indeed, accumulation of a dark intermediate (essential for detecting its TA features) is impossible when its formation is slower than its decay.

The GF analyses of the *ortho*- and *peri*-nitro derivatives required an introduction of infinity components, $\Delta A(\lambda, t = \infty)$, originating from transients with lifetimes significantly exceeding the dynamic range of the pump-probe technique. These long-lived species show broad weak TA that extends to 700 nm, and a peak at about 550 nm that overlaps with the ground-state bleach (Fig. 7E–H). The lack of nanosecond fluorescence signal from these compounds indicates that the $\Delta A(\lambda, t = \infty)$ transients correspond to dark states, *i.e.*, either to long-lived CT states responsible for the polarity-induced fluorescence quenching, or to triplets. Indeed, medium polarity enhances the formation of intramolecular CT states.[44] An increase in medium polarity, however, tends to decrease the ΔA amplitudes of these long-lived transients (Fig. 7E–H), precluding CT as the cause of their formation. Furthermore,

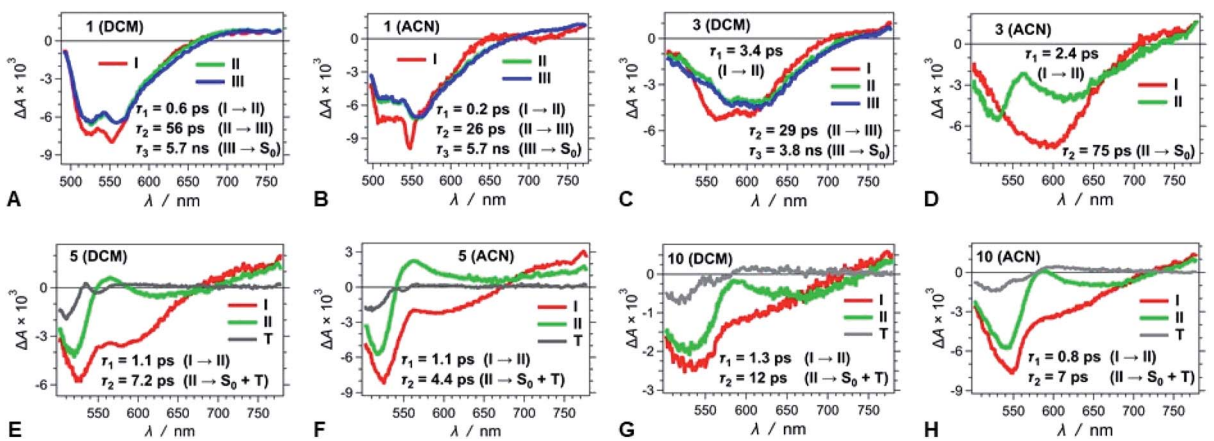

Fig. 7 TA spectra of (A–D) strongly fluorescent and (E–H) weakly and non-fluorescent DPNDs, depicting the transitions associated with the lifetimes, τ_i, obtained from GF analys.

placing nitro groups at *ortho* positions of phenyl substituents dramatically enhances the rates of ISC,[24] which is consistent with a triplet configuration in the long-lived transients that **5**, **6**, **7**, **10** and **11** produce.

While the TA analysis provided key insights about the excited-state dynamics of the DPNDs, there remained an open question as to the nature of the polarity-induced fluorescence quenching. Transitions through polar intermediates could explain the observed solvent-dependence trends. The rates of deactivation of such intermediates exceeding the rates of their formation, however, rendered them undetectable. Therefore, we resorted to computational studies to further elucidate the modes of deactivation the nitro-aryl substituted DPNDs.

Computational studies

Second-order Møller–Plesset (MP2)[45] perturbation theory allowed us to obtain *ab initio* estimates of the ground-state equilibrium geometries. For optimization of the excited states and evaluation of vertical excitation, we employed second-order algebraic diagrammatic construction, ADC(2).[46] The ADC(2) method provides a balanced description of intramolecular CT states, which makes it particularly advantageous for the analysis of organic nitro compounds.

For each of the dyes, the highest occupied molecular orbital (HOMO) and the lowest unoccupied molecular orbital (LUMO) involved in the lowest electronic transitions have, respectively, a π and π^* character, and are mainly localized on the DPND core (Fig. 8 and S69†). The radiative $\pi\pi^*$ transitions between the S_0 and S_1 states are strongly allowed, with oscillator strengths for optical absorption and emission close to unity (Fig. S69†). The computed energies for the vertical absorption and fluorescence agree well with the experimental results (Fig. S69†).

Removal of one nitrophenyl substituent from disubstituted DPNDs has a minor effect on their spectral properties, as a comparison between **3** and **8** illustrates (Fig. S69†). This finding agrees with the experimental results and with the localization of the radiative-transition NTOs on the DPND polycyclic ring system (Fig. 8 and S69†).

Despite this orbital localization on the DPND unit, a detailed analysis of the LUMOs shows their tendency to extend over the *ortho*- and *peri*-nitroaryl substituents. That is, optical excitation of these systems shifts some of the DPND electronic density to the nitroaryl moieties. While an increase in the dihedral angle between the aryl substituent and the DPND core slightly elevates the S_1 energy, it noticeably shortens the distance between one of the oxygens of the nitro group and the closest quaternary carbon on the pyrrole ring. Therefore, we follow this carbon–oxygen distance (R_{CO}) along the S_1 PES and compute the relaxed scans along it (blue squares, Fig. 9A. At a critical R_{CO} of about 2.4 Å, the PES of the $^1\pi\pi^*$ state crosses to the PES of another state (red triangles, Fig. 9A). This new state has a pronounced CT character as revealed by its NTOs (Fig. 9A), and the dipole moment of 3.93 D at the $^1\pi\pi^*$ equilibrium geometry rises to 10.95 D at $R_{CO} = 1.85$ Å.

As expected, the electron NTO of the ^{1}CT state localizes around the nitro group. Upon decreasing R_{CO}, however, there is a surprising density shift, leading to localization of the hole NTO around the pyrrole carbon and the nitro group (Fig. 9B). These changes prime the structure for covalent bonding between the pyrrole carbon and the nitro group oxygen. After passing through a small barrier at $R_{CO} \approx 2.2$ Å, a further decrease in R_{CO} stabilizes the ^{1}CT state (Fig. 9A and B). At $R_{CO} \approx 1.85$ Å, ^{1}CT crosses the PES of the ground state (Fig. 9A). This ^{1}CT/S_0 intersection provides a pathway for an efficient non-adiabatic transition to the ground state. These findings unequivocally confirm the conclusions from the spectroscopy studies, which indicate the involvement of a dark CT state in the non-radiative S_1 deactivation of the *ortho* and *peri* nitroaryl DPND derivatives.

At the geometry of the ^{1}CT/S_0 intersection, the formation of the carbon–oxygen covalent bond commences. Passing this intersection may lead to the formation of a photoproduct. A preferred trajectory in the ground state, involving the breaking of the temporarily-formed carbon–oxygen bond, however, restores the initial S_0 structure. In other words, an aborted photochemical reaction provides a channel for non-radiative decay of the S_1 state *via* internal conversion (IC).

The symmetric augmentation of the DPND core with two *ortho*-nitrophenyls in **10** raises the energy of the reactive ^{1}CT state with respect to the $^1\pi\pi^*$ one (Fig. S71, Tables S7 and S8†). The photochemical reaction breaks the molecular symmetry and polarizes the system. The dipole of 4.24 D in the $^1\pi\pi^*$ state increases to 6.51 D in the ^{1}CT state at $R_{CO} = 2.3$ Å, and doubles to 12.73 D as R_{CO} decreases to 1.85 Å.

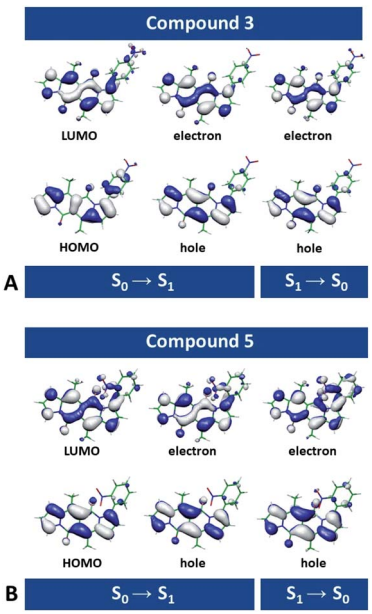

Fig. 8 Frontier and natural transition orbitals (NTOs) involved in the $S_0 \rightarrow S_1$ and $S_1 \rightarrow S_0$ radiative transitions, computed at the ADC(2)/cc-pVDZ level of theory for (A) **3** and (B) **5**. The long alkyl chains are truncated to methyls (isovalue = 0.03). The electron NTOs closely resemble the LUMOs, and the hole NTOs – the HOMOs. It is consistent with the HOMO → LUMO and LUMO → HOMO transitions providing the principal contributions to the absorption and the fluorescence.

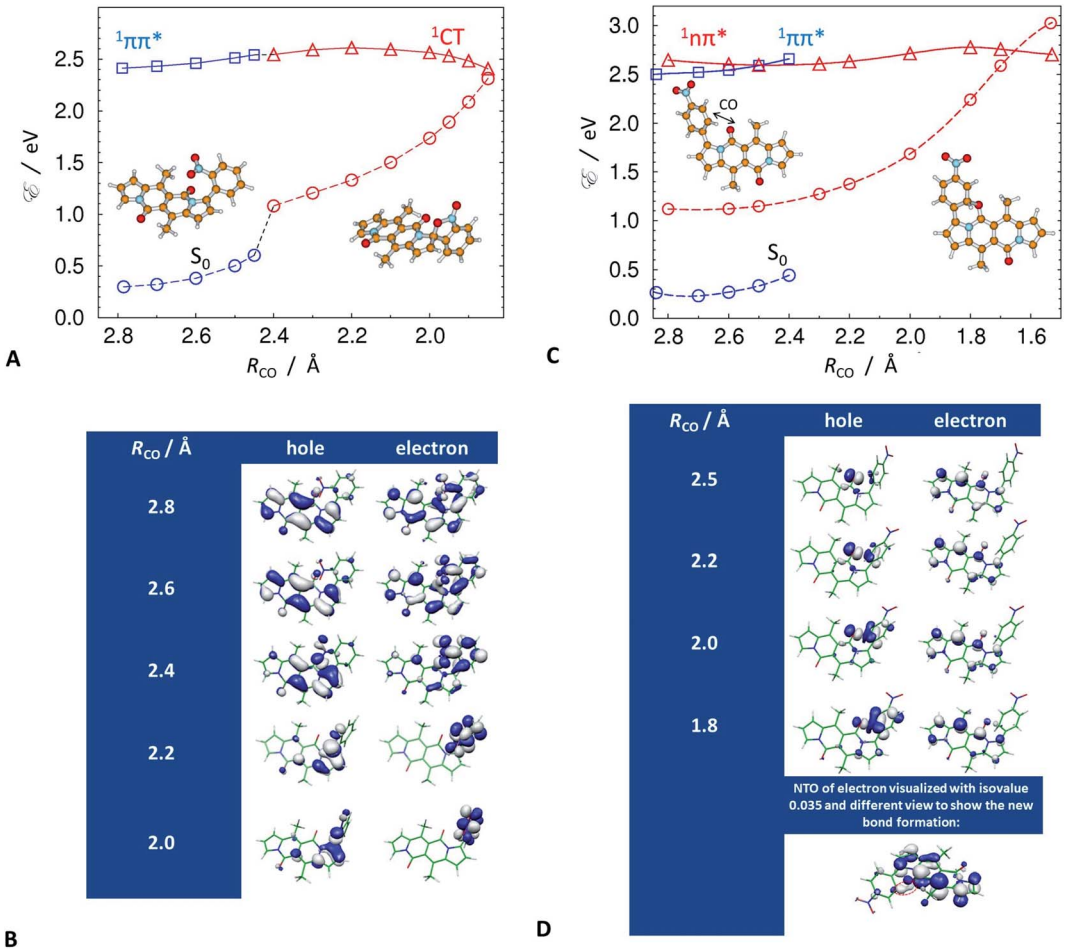

Fig. 9 Potential-energy profiles (PEPs) along the carbon–oxygen distances, R_{CO}, and the corresponding $S_1 \rightarrow S_0$ NTOs (isovalues = 0.03, unless indicated otherwise) optimized with the ADC(2)/def-SV(P) method in the lowest excited singlet states of (A and B) **5** and (C and D) **3**. (A and C) Circles connected by dashed line denote vertical energy of the ground state computed at the geometry of the respective excited state. For **5**, (A) locally-excited, $^1\pi\pi^*$, state – blue squares, and the dark charge-transfer, ^{1}CT, state – red triangles; and (B) NTOs along R_{CO}. For **3**, (C) locally-excited, $^1\pi\pi^*$, state – blue squares, and the dark $^1n\pi^*$ state – red triangles; and (D) NTOs along R_{CO}, where the last bottom structure depicts the electron NTO at isovalue of 0.035 to visualize the formation of the carbon–oxygen covalent bond, as circled with a red dashed line.

The same non-radiative decay channel operates in the *peri*-nitronaphthyl derivative, **7**, showing that the mechanism is not limited to just *ortho*-nitrophenyl conjugates. Furthermore, the naphthyl group provides additional stabilization to the reactive ^{1}CT state (Fig. S70†).

The *para* and *meta* derivatives, wherein the nitro groups are not as close to the DPND core, are not prone to forming such ^{1}CT states. Nonetheless, theoretical exploration of the PESs of the two lowest singlet excited states of **3**, and of the other strongly fluorescent nitroaryl DPNDs, reveals unexpected photoreactivity. At the S_0 geometry, S_1 and S_2 are $^1\pi\pi$ and $^1n\pi$ states, respectively, and the energy gap between them is relatively small, *i.e.*, on the order of 0.1 eV (Fig. 9C). An $S_0 \rightarrow {}^1n\pi^*$ optical transition is not dipole allowed. Nevertheless, vibronic coupling permits some intensity from the closely lying $^1\pi\pi^*$ state. All of the investigated compounds have this second-excited $^1n\pi^*$ state, regardless of the position of the nitro groups on the aryl substituents (Table S9†).

The optimized molecular structures show an elongation of the carbon–oxygen bond of the carbonyl group in the DPND core in the $^1n\pi^*$ state. On average, this bond length changes from 1.23 Å in the $^1\pi\pi^*$ state to 1.38 Å in $^1n\pi^*$ state, and brings the carbonyl oxygen close to the *ortho* carbons of the adjacent electron-deficient nitrophenyl substituent. We, therefore, selected this interatomic distance between the nitrophenyl carbon and the carbonyl oxygen to define R_{CO} for the analysis of the strongly fluorescent conjugates.

A decrease in R_{CO} destabilizes the $^1\pi\pi^*$ state and stabilizes the $^1n\pi^*$ state. Along R_{CO}, the potential-energy profiles (PEPs) of the lowest $\pi\pi^*$ and $n\pi^*$ singlet states of **3** cross at $R_{CO} = 2.5$ Å (Fig. 9C). Independent geometry optimization of different electronic states along a selected/distinguished intramolecular coordinate results in different their geometric displacements along the remaining 3N-7 intramolecular coordinates. In result one-dimensional potential-energy (PE) profiles plotted *vs.* selected reaction coordinate are differently displaced in remaining coordinates and their visualized

intersections are "apparent" (projected in 1-D). The real intersection between two PE profiles means that energies of both electronic states were computed at the same molecular geometry. The intramolecular coordinates of the $^1\pi\pi^*$ geometries differ from those of the $^1n\pi^*$ ones. The two vertical PEPs of the ground state, computed at these geometries, illustrate this difference (Fig. 9C).

The last stable point optimized in the $^1\pi\pi^*$ structure, at R_{CO} = 2.4 Å, represents an upper estimate of the barrier between the two excited states. Once the $^1n\pi^*$ state becomes S_1 and is populated, it has access to a conical intersection (CI) with S_0 at $R_{CO} \approx 1.7$ Å, protected by a barrier of about 0.2 eV at $R_{CO} \approx 1.8$ Å (Fig. 9C). The $^1n\pi^*/S_0$ CI provides a pathway for nonradiative deactivation of the S_1 state. Extension of the reaction pathway beyond the intersection with the ground state results in optimization of a metastable open-shell diradical structure. Concurrently, decreasing R_{CO} along the $^1n\pi^*$ PEP induces an increase in the NTO densities around the DPND carbonyl and the nitrophenyl (Fig. 9D). As a result, a non-nodal segment emerges in the electron NTO between the nitrophenyl carbon and the carbonyl oxygen.

While the $^1n\pi^*$ structures are not as polar as the ^{1}CT states of the *ortho* derivatives, an R_{CO} decrease still increases the S_1 dipole, *e.g.*, for **3**, μ_{S1} = 3.53 D at R_{CO} = 2.5 Å, and μ_{S1} = 6.93 D at R_{CO} = 1.8 Å. Therefore, an increase in solvent polarity stabilizes the $^1n\pi^*$ structures with reduced R_{CO} more than it does the locally excited (LE) $^1\pi\pi^*$ state, which lowers the barriers along the S_1 PES and favours the non-radiative transition through the $^1n\pi^*/S_0$ CI. This finding is consistent with the polarity-induced quenching of the emission of even the strongly fluorescent nitroaryl conjugates, except of **13** where the nitro group is practically completely decoupled from the DPND core (Fig. 4D and F).

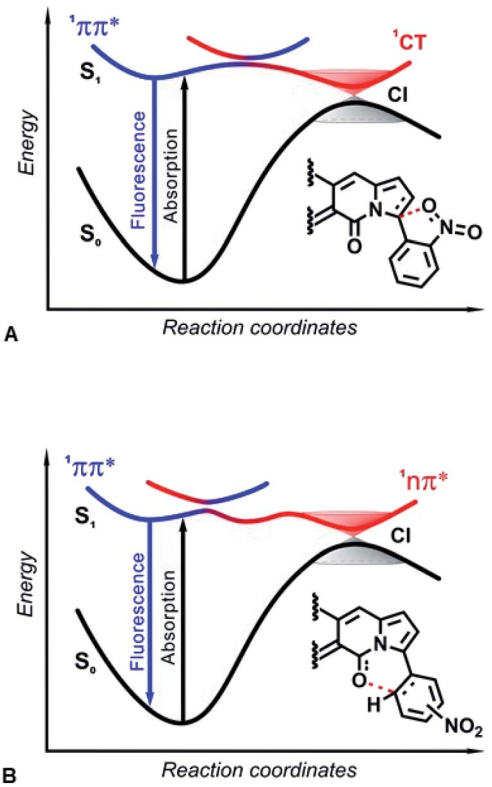

Fig. 10 Excited-state dynamics of nitroaryl-substituted DPNDs. The formed LE $^1\pi\pi^*$ states either radiatively decay to S_0, or non-adiabatically transfer to dark states that form CIs with S_0 providing pathways for non-radiative deactivation. (A) Placing the nitro groups close to the DPND core, such as in the *ortho* and *peri* derivatives, accommodates the formation of dark CT states and the non-radiative deactivation assumes a $^1\pi\pi^* \rightarrow {}^1$CT $\rightarrow S_0$ pathway. (B) When the nitro groups are not spatially close to the DPND core, such as in the *para* and *meta* derivatives, the energy level of the FC second singlet excited state, with a $^1n\pi^*$ character, decreases along the reaction coordinate, opening a $^1\pi\pi^* \rightarrow {}^1n\pi^* \rightarrow S_0$ pathway for non-radiative deactivation.

Discussion

Efficient ISC, involving $^1\pi\pi^*$ and $^1n\pi^*$ singlet and triplet states, is one of the most prevalent reasons why nitro compounds do not fluoresce. The high density of triplet states and closely situated singlet excited states with $^1\pi\pi^*$ and $^1n\pi^*$ character ensure non-radiative decay *via* ISC. Photophysical and computational studies of nitroaryl DPNDs reveal for the first time how the two lowest $^1\pi\pi^*$ and $^1n\pi^*$ singlet excited states, on their own, can provide a pathway for non-radiative deactivation. This mechanism of decay through a dark $^1n\pi^*$ state is universal for all nitroaryl DPNDs under study, and the threshold for such non-radiative deactivation channels depends on the energy gap between the $^1\pi\pi^*$ and $^1n\pi^*$ states (Table S9†).

When other channels dominate the non-radiative deactivation, the $^1\pi\pi^* \rightarrow {}^1n\pi^* \rightarrow S_0$ mechanism is undetectable, as the *ortho* and *peri* derivatives reveal, where ISC and a transition through a dark ^{1}CT state are responsible for the fluorescence quenching. Orthogonality of *ortho*-nitrophenyl substituents with the DPND core fosters states with strong spin–orbit coupling that have negligible dependence on the solvent polarity.[24] Polar environments, however, stabilize the highly polarized CT states considerably more than they do the less polar $^1\pi\pi^*$ states, resulting in the observed enhancement of k_{nr} (Fig. 4F and Table S2†).

In both IC decay mechanisms, the reactivity of the $^1n\pi^*$ and ^{1}CT states induces a temporary formation of covalent bonds along the S_1 PESs toward the CIs. Ultimately, these covalent bonds break upon relaxation to the ground state (Fig. 10). Based on *ab initio* calculations, in the 1990s Domcke and Sobolewski proposed the concept of a low-barrier photoreaction pathway interrupted by a CI with the ground state as a mechanism for ultrafast excited-state deactivation.[31] Such photochemical reactions, aborted at CIs between the PESs of S_1 and S_0 states, offer efficient channels for ultrafast IC, leading to recovery of the reactant after photoexcitation.[47] For example, the quenching of deleterious photochemical reactions by ultrafast IC is important for the high intrinsic photostability of DNA bases as well as sugars and peptides.[48–50] Herein, interactions of the nucleophilic oxygens of the nitro group (and the DPND carbonyls) with electrophilic carbons of the pyrroles (and the nitroaryl substituents) present a key paradigm for fluorescence quenching *via* aborted photochemistry (Fig. 10).

Conclusions

Weakening the electron-donating capabilities of a DPND chromophore core while balancing its coupling with nitro groups attached to its aryl substituents produces fluorescent compounds. Many of these dyes sustain their emission in polar solvents, unlike other nitroaromatics. The implemented molecular designs suppress modes of non-radiative decay that are common in nitroaromatic compounds. This suppression leads to the emergence of alternative pathways of non-radiative deactivation involving aborted photochemistry. Along with dihedral degrees of freedom, the nucleophilic oxygens and electrophilic carbons of nitroaryl derivatives render such compounds prone to intramolecular photochemical reactions. When conical intersections interrupt the trajectories of these reactions, internal conversion leads to restoration of the initial ground state and molecular structure. This sequence of processes represents a completely unexplored mechanism for the non-radiative deactivation of nitroaromatics. These results set a key photophysical paradigm, providing important guidelines for the design and engineering of new classes of fluorescent nitroaromatics.

Data availability

Data associated with this article, including experimental procedures, compound characterization, steady-state absorption and emission along with the time-resolved pump-probe transient absorption details and computational analysis details are available in the ESI.†

Author contributions

B. S., D. T. G. and P. P. conceived the project; B. S. designed, synthesized and characterized all nitroaromatics; P. P. carried out time-integrated and time-resolved spectroscopic studies, analyzed and interpreted spectroscopic results; M. K., Y. M. P., M. C., P. J., T. D. L. and M. B. performed physicochemical investigation; J. A. C. analyzed the transient absorption results; A. L. S. conducted the computational studies; W. G. and D. M. and helped in the conduction of the project; B. K., M. Ł. and V. I. V. co-directed the project; V. I. V. was instrumental in writing the final version of the manuscript. All authors contributed to writing the manuscript.

Conflicts of interest

There are no conflicts to declare.

Acknowledgements

The work was financially supported by the Polish National Science Centre, Poland (PRELUDIUM 2016/23/N/ST5/00054, HARMONIA 2016/22/M/ST5/00431, 2017/25/B/ST5/02488 to P. J. and SONATA 2017/26/D/ST3/00910 to P. P.), the Foundation for Polish Science (TEAM POIR.04.04.00-00-3CF4/16-00 and START scholarship no. 076.2020 to B. S.), the Polish National Agency for Academic Exchange (fellowship to B. S. within the Bekker programme PPN/BEK/2019/1/00256), the USA National Science Foundation (grant number CHE 1800602, and AGEP supplement supporting J. A. C.), the American Chemical Society Petroleum Research Fund (grant number 60651-ND4), the USA National Institutes of Health, National Eye Institute (grant R01 EY027440) and European Commission (CHAIR 860762). We extend our gratitude to Dr Simon J. Teat for training and guidance through our crystallography studies at the Advanced Light Source (ALS), Lawrence Berkeley National Laboratory, supported by the Office of Science, Office of Basic Energy Sciences, of the U.S. Department of Energy under Contract No. DE-AC02-05CH11231.

Notes and references

1 M.-C. Chen, D.-G. Chen and P.-T. Chou, *ChemPlusChem*, 2021, **86**, 11–27.
2 D. J. Cowley, *Helv. Chim. Acta*, 1978, **61**, 184–197.
3 B. Bursa, D. Wróbel, B. Barszcz, M. Kotkowiak, O. Vakuliuk, D. T. Gryko, Ł. Kolanowski, M. Baraniak and G. Lota, *Phys. Chem. Chem. Phys.*, 2016, **18**, 7216–7228.
4 N. I. Rtishchev, D. V. Samoilov, V. P. Martynova and A. V. El'tsov, *Russ. J. Gen. Chem.*, 2001, **71**, 12.
5 E. F. Plaza-Medina, W. Rodríguez-Córdoba and J. Peon, *J. Phys. Chem. A*, 2011, **115**, 9782–9789.
6 Z. Cheng, E. Kuru, A. Sachdeva and M. Vendrell, *Nat. Rev. Chem.*, 2020, **4**, 275–290.
7 A. Morozumi, M. Kamiya, S. Uno, K. Umezawa, R. Kojima, T. Yoshihara, S. Tobita and Y. Urano, *J. Am. Chem. Soc.*, 2020, 0c00451.
8 T. M. Wilson, M. J. Tauber and M. R. Wasielewski, *J. Am. Chem. Soc.*, 2009, **131**, 8952–8957.
9 M. Stolar and T. Baumgartner, *Phys. Chem. Chem. Phys.*, 2013, **15**, 9007.
10 Q. Yue, W. Liu and X. Zhu, *J. Am. Chem. Soc.*, 2020, **142**, 11613–11628.
11 A. Ashcraft, K. Liu, A. Mukhopadhyay, V. Paulino, C. Liu, B. Bernard, D. Husainy, T. Phan and J.-H. Olivier, *Angew. Chem., Int. Ed.*, 2020, **59**, 7487–7493.
12 K. Skonieczny, I. Papadopoulos, D. Thiel, K. Gutkowski, P. Haines, P. M. McCosker, A. D. Laurent, P. A. Keller, T. Clark, D. Jacquemin, D. M. Guldi and D. T. Gryko, *Angew. Chem., Int. Ed.*, 2020, **59**, 16104–16113.
13 T. Ueno, Y. Urano, H. Kojima and T. Nagano, *J. Am. Chem. Soc.*, 2006, **128**, 10640–10641.
14 J.-M. Mewes, V. Jovanović, C. M. Marian and A. Dreuw, *Phys. Chem. Chem. Phys.*, 2014, **16**, 12393–12406.
15 C. E. Crespo-Hernández, G. Burdzinski and R. Arce, *J. Phys. Chem. A*, 2008, **112**, 6313–6319.
16 J. S. Zugazagoitia, C. X. Almora-Díaz and J. Peon, *J. Phys. Chem. A*, 2008, **112**, 358–365.
17 E. F. Plaza-Medina, W. Rodríguez-Córdoba, R. Morales-Cueto and J. Peon, *J. Phys. Chem. A*, 2011, **115**, 577–585.
18 J. P. Zobel, J. J. Nogueira and L. González, *Chem.–Eur. J.*, 2018, **24**, 5379–5387.

19 S. Saha and A. Samanta, *J. Phys. Chem. A*, 1998, **102**, 7903–7912.
20 P. B. Ghosh and M. W. Whitehouse, *Biochem. J.*, 1968, **108**, 155–156.
21 S. Benson, A. Fernandez, N. D. Barth, F. de Moliner, M. H. Horrocks, C. S. Herrington, J. L. Abad, A. Delgado, L. Kelly, Z. Chang, Y. Feng, M. Nishiura, Y. Hori, K. Kikuchi and M. Vendrell, *Angew. Chem., Int. Ed.*, 2019, **58**, 6911–6915.
22 R. López-Arteaga, A. B. Stephansen, C. A. Guarin, T. I. Sølling and J. Peon, *J. Phys. Chem. B*, 2013, **117**, 9947–9955.
23 M.-C. Chen, Y.-L. Lee, Z.-X. Huang, D.-G. Chen and P.-T. Chou, *Chem.–Eur. J.*, 2020, **26**, 7124–7130.
24 Y. M. Poronik, G. V. Baryshnikov, I. Deperasińska, E. M. Espinoza, J. A. Clark, H. Ågren, D. T. Gryko and V. I. Vullev, *Commun. Chem.*, 2020, **3**, 190.
25 D. H. Friese, A. Mikhaylov, M. Krzeszewski, Y. M. Poronik, A. Rebane, K. Ruud and D. T. Gryko, *Chem.–Eur. J.*, 2015, **21**, 18364–18374.
26 Ł. G. Łukasiewicz, H. G. Ryu, A. Mikhaylov, C. Azarias, M. Banasiewicz, B. Kozankiewicz, K. H. Ahn, D. Jacquemin, A. Rebane and D. T. Gryko, *Chem.–Asian J.*, 2017, **12**, 1736–1748.
27 M. Tasior, G. Clermont, M. Blanchard-Desce, D. Jacquemin and D. T. Gryko, *Chem.–Eur. J.*, 2019, **25**, 598–608.
28 Z. Szakács, M. Tasior, D. T. Gryko and E. Vauthey, *ChemPhysChem*, 2020, **21**, 1718–1730.
29 B. Dereka, A. Rosspeintner, M. Krzeszewski, D. T. Gryko and E. Vauthey, *Angew. Chem., Int. Ed.*, 2016, **55**, 15624–15628.
30 M. Grzybowski, I. Deperasińska, M. Chotkowski, M. Banasiewicz, A. Makarewicz, B. Kozankiewicz and D. T. Gryko, *Chem. Commun.*, 2016, **52**, 5108–5111.
31 A. L. Sobolewski, C. Woywod and W. Domcke, *J. Chem. Phys.*, 1993, **98**, 5627–5641.
32 I. J. Palmer, I. N. Ragazos, F. Bernardi, M. Olivucci and M. A. Robb, *J. Am. Chem. Soc.*, 1993, **115**, 673–682.
33 W. Domcke and A. L. Sobolewski, *Science*, 2020, **368**, 820–821.
34 J. Yang, X. Zhu, J. P. F. Nunes, J. K. Yu, R. M. Parrish, T. J. A. Wolf, M. Centurion, M. Gühr, R. Li, Y. Liu, B. Moore, M. Niebuhr, S. Park, X. Shen, S. Weathersby, T. Weinacht, T. J. Martinez and X. Wang, *Science*, 2020, **368**, 885–889.
35 B. Sadowski, M. F. Rode and D. T. Gryko, *Chem.–Eur. J.*, 2018, **24**, 855–864.
36 B. Sadowski, M. Loebnitz, D. R. Dombrowski, D. H. Friese and D. T. Gryko, *J. Org. Chem.*, 2018, **83**, 11645–11653.
37 L. Wang, L. Lin, J. Yang, Y. Wu, H. Wang, J. Zhu, J. Yao and H. Fu, *J. Am. Chem. Soc.*, 2020, **142**, 10235–10239.
38 B. Sadowski, S.-H. Su, T.-C. Lin, T. D. Lohrey, I. Deperasińska, P.-T. Chou and D. T. Gryko, *J. Mater. Chem. C*, 2018, **6**, 12306–12313.
39 G. Jones, D. Yan, J. Hu, J. Wan, B. Xia and V. I. Vullev, *J. Phys. Chem. B*, 2007, **111**, 6921–6929.
40 A. L. Thompson, T.-S. Ahn, K. R. J. Thomas, S. Thayumanavan, T. J. Martínez and C. J. Bardeen, *J. Am. Chem. Soc.*, 2005, **127**, 16348–16349.
41 N. Mataga, Y. Kaifu and M. Koizumi, *Bull. Chem. Soc. Jpn.*, 1956, **29**, 465–470.
42 E. Lippert, *Zeitschrift für Naturforschung A*, 1955, **10**, 541–545.
43 Y. Ooshika, *J. Phys. Soc. Jpn.*, 1954, **9**, 594–602.
44 J. B. Derr, J. Tamayo, J. A. Clark, M. Morales, M. F. Mayther, E. M. Espinoza, K. Rybicka-Jasińska and V. I. Vullev, *Phys. Chem. Chem. Phys.*, 2020, **22**, 21583–21629.
45 C. Møller and M. S. Plesset, *Phys. Rev.*, 1934, **46**, 618–622.
46 A. B. Trofimov and J. Schirmer, *J. Phys. B: At., Mol. Opt. Phys.*, 1995, **28**, 2299–2324.
47 I. Schapiro, F. Melaccio, E. N. Laricheva and M. Olivucci, *Photochem. Photobiol. Sci.*, 2011, **10**, 867.
48 A. Sinicropi, W. M. Nau and M. Olivucci, *Photochem. Photobiol. Sci.*, 2002, **1**, 537–546.
49 D. Tuna, A. L. Sobolewski and W. Domcke, *Phys. Chem. Chem. Phys.*, 2014, **16**, 38–47.
50 D. Shemesh, A. L. Sobolewski and W. Domcke, *J. Am. Chem. Soc.*, 2009, **131**, 1374–1375.